Journal of Applied Polymer Science

The Influence of $Cu_3(BTC)_2$ metal organic framework on the permeability and perm-selectivity of PLLA-MOF mixed matrix membranes

Ajay Kathuria,[1] Saleh Al-Ghamdi,[2,3] Mohamad G. Abiad,[2,4] Rafael Auras[2]

[1]Industrial Technology and Packaging, California Polytechnic State University, San Luis Obispo, California 93407

[2]School of Packaging, Packaging Building Michigan State University, East Lansing, Michigan 48824-1223

[3]Department of Agricultural Engineering, College of Food and Agricultural Sciences, King Saud University, Riyadh 11451, Saudi Arabia

[4]Department of Nutrition and Food Sciences, American University of Beirut, Riad El Solh, Beirut 1107-2020, Lebanon

Correspondence to: A. Kathuria (E-mail: akathuri@calpoly.edu)

ABSTRACT: Poly(L-lactic acid) (PLLA) - 20% (w/w) and $Cu_3(BTC)_2$ metal organic framework (MOF) based mixed matrix membranes (MMMs) were fabricated by a vertical corotating twin screw microcompounder followed by an injection molding process. Water vapor, CO_2, O_2, and selected aroma mass transfer properties of PLLA and PLLA MMMs were evaluated. The CO_2/O_2 perm-selectivity of PLLA ($\alpha_{CO2/O2}$) MMMs increased from 7.6 to 10.3 with the incorporation of 20% $Cu_3(BTC)_2$ MOF. Gravimetric permeability studies of trans-2-hexenal performed at 23°C and 50% RH indicated that permeability coefficient of PLLA MMMs increased by around 60% as compared to regular PLLA film. However, no changes in mass transfer rates were observed for acetaldehyde. Furthermore, the thermal processing parameters as well as the presence of MOF did not show any significant effect on the molecular weight of the PLLA matrix nor on the crystalline structure of the $Cu_3(BTC)_2$ MOF, which was confirmed by both gel permeation chromatography and X-ray diffraction studies. © 2015 Wiley Periodicals, Inc. J. Appl. Polym. Sci. **2015**, *132*, 42764.

KEYWORDS: biomaterials; composites; membranes; morphology; packaging

Received 16 May 2015; accepted 21 July 2015

DOI: 10.1002/app.42764

INTRODUCTION

Poly(lactic acid) (PLA) has increased its market presence in the packaging and the textile industries due to growing environmental awareness and competitive resin prices. Permeability of various gases, water molecules, and organic compounds play an important role in the selection of polymeric membranes for industrial applications such as separation, bioremediation, and food and medical packaging. PLA is a reasonably good permeability for carbon dioxide (CO_2) and water vapor as compared to traditional petroleum based polymers like poly(vinyl chloride), poly(ethylene terephthalate), and poly(propylene), which can be a positive attribute for respiring products.[1–3] The thermal, mechanical and barrier properties of PLA are significantly affected by its isomeric composition (i.e., PLLA or PDLA content) and crystallinity.[4–6] Tsuji and Tsuruno[6] reported that PLLA/PDLA blend films with only stereocomplex crystallites had lower water permeability coefficients than PLLA or PDLA polymers alone.

Metal organic frameworks (MOFs), a class of micro-porous materials, have attracted a lot of attention due to their high adsorption properties, catalysis, high surface area, and bactericidal activities.[7–10] MOFs can host various molecules in their pores depending on their interaction, pore size, and volume. The host-guest interactions between MOFs and gaseous, water vapors or organic molecules have been credited to: (i) the available metal sites, which interact/coordinate with the gases or water molecules and (ii) organic linkers which can physically adsorb gases due to secondary forces.[11–13] The ability of a specific MOF to host or interact with particular type gas molecules depends on the various factors such as: type of the organic linkers present in the MOF structure, number of aromatic rings present in the organic linker, and type of the functional groups attached to the organic linkers or metal species. Therefore, for a given application, proper selection of a MOF is key to obtain the desired sorption, selectivity and gas separation.

A membrane can be defined as a physical barrier, which allows selective transport of molecules. The effectiveness of a membrane can be judged from its permeability and selectivity. Along with high selectivity, reasonably good permeable membrane is required

to achieve high productivity. Permeability coefficient (P) of a membrane is dependent on the solubility (S) and diffusion (D) coefficients and can be mathematically calculated using eq. (1).

$$P = D \times S = \frac{q \times l}{A \times t \times \Delta p} \quad (1)$$

where, q is amount of the permeant transferred through the membrane, l is thickness of the membrane, A is surface area, t is time, and Δp is the pressure differential between the two sides of the membrane. Selectivity (α) can be measured by the ratio of the permeability of a gas A over the permeability coefficient of another gas B.

In this research, copper benzene 1,3,5 tricarboxylate $Cu_3(BTC)_2$ MOF was selected for its ability to interact with CO_2.[14] Membranes with high perm-selectivity for CO_2 gas can be used in various industrial applications, which include capturing greenhouse gases, separating CO_2/CH_4 to obtain high calorific methane for gas, etc. In packaging, these membranes can be used to selectively remove gases or aromatic molecules and to maintain optimum concentration of CO_2, organic compounds, or other gases in the headspace of a package, which can impact the package performance.

Kusgen *et al.*[15] characterized $Cu_3(BTC)_2$ MOF using water adsorption. They suggested that water adsorption follows two steps: (i) axial coordination of the water molecules to the polar hydrophilic copper sites and (ii) filling of non-polar hydrophobic sites due to organic linkers at higher pressure. Castillo *et al.*,[16] studied the interaction of various hydrocarbons, gaseous, and water molecules using *Monte Carlo* molecular simulation, found that $Cu_3(BTC)_2$ MOF has strong adsorption and affinity toward water molecules compared with other gaseous molecules in the following order $CO_2 > O_2 > N_2$. This indicates that during an application water molecules will compete with other gases for available sites. Supronowicz *et al.*[17] calculated the adsorption energies of H_2O, CO_2, and O_2, among other gaseous molecules, using *ab initio* density functional theory. The adsorption enthalpies for H_2O, CO_2, and O_2 calculated in this study were −53.8, −20.1, and −5.7 kJ/mol, respectively. The higher water adsorption enthalpy can be supported by the formation of a reversible coordinate bond between the free metal sites and the water molecules. These studies have also highlighted the existence of good Van der Waals interactions between $Cu_3(BTC)_2$ MOF and CO_2 molecules.[15–17]

Mixed matrix membranes (MMMs) generally consist of a continuous polymeric matrix and filler that can enhance the performance of the polymeric membranes. It has been demonstrated that the presence of mesoporous or microporous fillers such as zeolites,[18,19] carbon molecular sieves,[20] and MOFs[21,22] can increase the gas permeability and enhance the separation properties of these polymeric matrices. However, MOFs have been the focus in the last decade for their ease of synthesis, high surface area, gas selectivity, and adsorption.[23] The hybrid organic-inorganic compositions of the MOFs renders them good candidates for polymer based MMMs since such hybrid compounds can offer defect free MMMs with good thermal stability.[24–26]

In previous studies,[24,27] we demonstrated that PLLA and $Cu_3(BTC)_2$ MOF have strong interfacial interactions. We have also established that using melt extrusion we can prepare defect free PLA-$Cu_3(BTC)_2$ MOF composites.[27] The purpose of this study is to understand the effect of $Cu_3(BTC)_2$ MOF on the H_2O, CO_2, O_2, trans-2-hexenal, and acetaldehyde mass transfer and perm-selectivity in the PLLA matrix for potential use of MMMs in industrial applications such as gas separation and packaging. Organic aroma compounds such as trans-2-hexenal and acetaldehyde generally exist in fresh produce and their presence is related to the freshness and acceptance of the food product. For this reason, the mass transfer properties of PLLA-$Cu_3(BTC)_2$ MOF based MMMs for various gases and vapors have been evaluated.

METHODOLOGY

Materials

Poly(L-lactic acid) (PLLA) grade 4043 D with 98% L-lactide content was provided by NatureWorks LLC (Minnetonka, MN). PLLA resin has an average molecular weight (M_w), number average molecular weight (M_n), and polydispersity index (M_w/M_n) of 111 kDa, 84 kDa, and 1.3, respectively. Basolite™ C300 MOF [Cu_3 BTC_2] with a surface area ranging from 1500 to 2100 m^2 g^{-1} and particle size varying between 5 and 30 μm was purchased from Sigma Aldrich (St. Louis, MO). Trans-2-hexenal (purity ≥95%) was supplied by SAFC. Acetaldehyde [purity ≥99%] was purchased from Sigma-Aldrich Corp (St. Louis, MO). Acetaldehyde and trans-2-hexenal were both stored at 5°C prior use.

Fabrication of the PLLA-Mof Membranes

PLLA resin was dried for 4 h at 80°C and Basolite™ C 300 MOF was activated at 200°C and 4 kPa (30 mmHg) for 24 h using a vacuum oven. PLLA and PLLA-20% MOF composite samples were processed using a vertical corotating twin-screw microcompounder (DSM Research, Geleen, The Netherlands) attached to an injection molder. The extruder has 150 mm long screws with length to diameter ratio of 18 and a barrel volume of 15 cm^3. The material was processed at 190°C using 5 min cycle time at ~1 MPa (140 psi) injection pressure. The transfer cylinder and mold temperatures were set at 195 and 65°C, respectively. X-ray diffraction (XRD) discs of PLLA and PLLA-20% activated MOF composites were prepared and stored in a desiccator at room conditions of 23 ± 0.1°C.

The injection molded samples were then compressed into films at 170°C and ~1.0 MPa for 5 min using a PHI 30 ton compression molding machine (City of industry, CA) equipped with 12 × 12″ in plate.

Surface Area and Pore Volume Measurement

$Cu_3(BTC)_2$ MOF specimens were examined using a Nova 2200 (Quantachrome Instruments, Boynton Beach, FL) gas sorption analyzer with N_2 gas. The porous material $Cu_3(BTC)_2$ was activated by placing ~5 mg in the outgassing station for 24 h at 200°C (heating rate of 10°C/min) under vacuum 0.1333 kPa (1 torr). After activation, the samples were loaded in the physisorption station. The sorption isotherm at −195.85°C (77.3 K) was determined for relative pressure (P/P_o) varying from 10^{-6}

to 0.99 followed by desorption to 0.05 P/P_o. The surface area was determined using the Brunauer-Emmett-Teller (BET) method and obtained from very small relative pressure $P/P_o < 0.05$. The total pore volume was calculated using eq. (2).

$$V_p = \frac{W_a}{\rho_l} \quad (2)$$

where, V_p is the total pore volume, W_a the adsorbed amount (grams of nitrogen to specimen amount in grams), and ρ_l the density of nitrogen.

Scanning Electron Microscopy (SEM)

$Cu_3(BTC)_2$ MOF and PLLA-20% MOF composite samples were sputter gold coated to avoid any charging on these materials. The SEM images of MOF particles were captured using JEOL JSM 6400 SEM equipped with tungsten filament at 12 kV accelerating voltage. The morphology of the composites was analyzed using Philips Quanta 200 ESEM operated in low vacuum mode at a chamber pressure of 90 Pa and acceleration voltage of 10 kV accelerating voltage.

X-ray Diffraction

XRD analysis was performed on XRD discs of PLLA, $Cu_3(BTC)_2$ MOF, and PLLA-20% MOF stored at 23°C using a Bruker D8 advance X-ray diffractometer (Bruker AXS GmgH, Karlsruhe, Germany) at 40 kV, 40 mA (1,600 W) using Cu Kα radiation ($\lambda = 1.5418$ Å). The studies were conducted using a 1.2 mm primary beam slit and 2.0 mm detector slit. The X-ray scans were carried out at a speed of 0.02°/s. Specimens were run in triplicates.

Mass Transfer Properties

Carbon Dioxide Transmission Rate (CO_2TR). CO_2TR of the PLLA and PLLA-20% MOF were measured as per ASTM F2476-05 using a Permatran® 4/41 (MOCON, Minneapolis, MN) at 23°C and 0% RH using 100% CO_2. N_2 was used as a carrier gas at a flow rate of 50 sccm. The data points were collected every 30 min until stable saturated state was achieved. The transmission rate of film ranging from 4 to 6 mil thickness was measured using an aluminum mask with 3.14 cm^2 area. The average value of the last 10 stable points in steady state was used to calculate the permeability values using eq. (3). The data were analyzed for at least three samples.

$$\text{Permeability Coefficient} = \frac{\text{transmission rate}\,(\text{kg m}^{-2}\text{s}^{-1}) \times \text{thickness}\,(\text{m})}{\text{pressure differential}\,(\text{Pa})} \quad (3)$$

Oxygen Transmission Rate (OTR). The OTRs of the PLLA and PLLA-20% MOF were measured as per ASTM D3985-05 using an Oxtran® 2/21 (MOCON., Minneapolis, MN) at 23°C and 0% RH using 100% oxygen gas as permeant and 98% N_2/2% H_2 as the carrier gas at a flow rate of 20 sccm of the test gas and 10 sccm flow rate of carrier gas. The data was collected every 30 min until stable saturated state was achieved. The transmission rate of 4–6 mil thick films was measured using aluminum masks with 3.14 cm^2 area. The average value of the last ten stable points was used to calculate the permeability values using eq. (3). The data were analyzed for at least three samples.

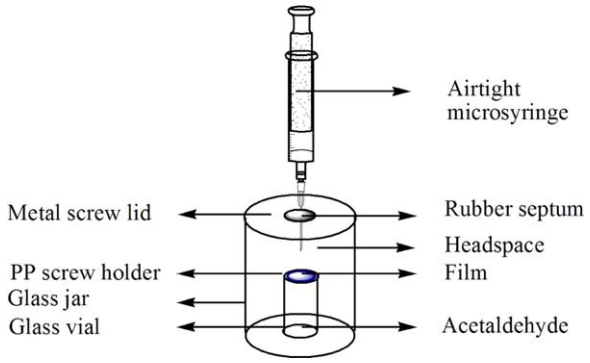

Figure 1. Schematic representation of experimental set up for permeability studies of acetaldehyde using gas chromatograph. [Color figure can be viewed in the online issue, which is available at wileyonlinelibrary.com.]

Water Vapor Transmission Rate (WVTR). The WVTRs of the PLLA and PLLA-20% MOF were measured according to ASTM F1249 using a Permatran® W3/31 (MOCON, Minneapolis, MN) at 23°C and 100% RH with N_2 gas having 0% RH as a carrier at a flow rate of 100 sccm. The data was collected using exam time of 30 min until stable saturated state was achieved. The transmission was measured using aluminum masks with a film area of 3.14 cm^2. The average value of last 10 stable points was used to calculate the permeability values using eq. (3). The data were collected in triplicates.

Aroma Permeability Coefficient. Due to the volatile nature of acetaldehyde (C_2H_4O) and its low boiling point, the permeation was measured at 0% RH in a cooling chamber (PTC-1 Temperature Cabinet, NA) at 10.0 ± 0.25°C with controller device (Sable System International, NA). The quasi-isostatic permeation experiment was simulated by placing a 4 mL vial filed with 300 µL of acetaldehyde and sealed with polypropylene (PP) screw holder with PLLA or PLLA-20% MOF membranes inside a 2 L glass jar as shown in Figure 1. The PP screw cap exposed 0.5 cm^2 surface area of the film. Acetaldehyde was allowed to adsorb, and diffuse through, the PLLA and PLLA-20% MOF from the 4 mL vial to the 2 L glass jar. Accumulation of acetaldehyde was measured by drawing 25 µL gas from the headspace of the glass jar and injected it in a gas chromatography (GC; Hewlett Packard GC 6890, CA), at 15 min, 1, 2, 3, 4, 12, 24, 36, 48, 60, and 72 h for each replicate.

A calibration curve was constructed prior this study by injecting acetaldehyde from the jar using a Pressure-Lok© syringe from Sigma-Aldrich (St. Louis, MOA) ranging from 1 to 300 µL repeated in three replicates after incubation for 24 and 72 h at 10°C. The injection temperature was 40°C, the cycle was conducted at 40 to 240°C. The initial time was 2 min and the heating ramp was 10°C min^{-1}. The gas flow was 30 mL min^{-1}.

The aroma vapor transmission rate of trans-2-hexenal ($C_6H_{10}O$) was measured using a modified ASTM E-96 cup method at 23 ± 0.1°C, 50 ± 2% RH and partial pressure difference of 1.436 kPa. The aroma vapor permeability coefficients of the PLLA and PLLA-20% MOF were calculated from the

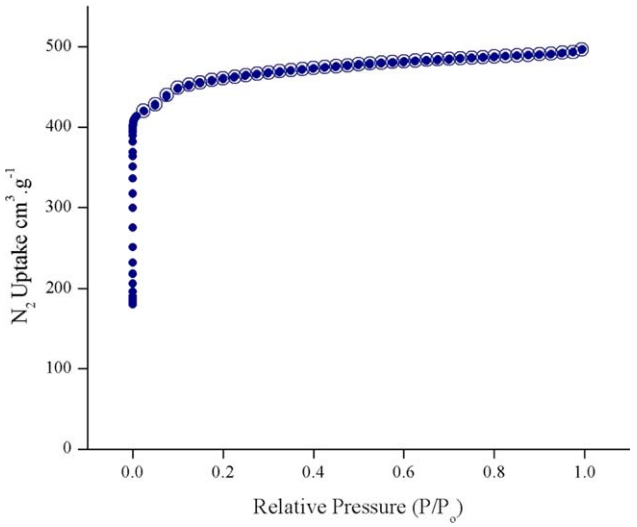

Figure 2. Nitrogen sorption (closed circles)-desorption (opened circles) isotherm of $Cu_3(BTC)_2$ MOF. [Color figure can be viewed in the online issue, which is available at wileyonlinelibrary.com.]

slope of the weight loss from the cup with respect to time using eq. (4).

aroma permeability

$$= \frac{\text{slope (kg/s)} \times \text{thickness (m)}}{\text{partial pressure difference (Pa)} \times \text{area (m}^2\text{)}} \quad (4)$$

Gel Permeation Chromatography (GPC)

GPC, Waters (Milford, MA), was used to study the effect of processing parameters on the molecular weight of the PLLA and PLLA-MOF composites. The instrument was calibrated using polystyrene standards with molecular weight ranging from 2.9×10^3 to 3.64×10^6 Da using a third order polynomial equation. The tests were conducted at a flow rate of 1 mL min^{-1} and runtime of 45 min at 35°C using the Mark-Houwink corrected constant $K = 0.000174$ (mL g^{-1}) and $a = 0.736$ for dilute PLLA solution in tetrahydrofuran (THF).[28] The instrument was equipped with a Waters 1515 isocratic pump, Waters 717 auto-sampler, a series of Waters Styragel Columns (HR4, HR3, and HR2) and Waters 2414 refractive index. To perform the GPC studies, ~20 mg of material was dissolved in 10 mL of HPLC grade THF with 99.99% purity (Pharmco-Aaper, Brookfield, CT). The solution was then filtered using a 0.45 μm filter.

Data Analysis

Tukey's HSD (Honestly Significant Differences) tests were performed to determine if the means were significantly different from each other at a 95% confidence interval ($\alpha = 0.05$). The analyses were conducted using SAS 9.0 and 9.4 software (SAS Institute, Cary, NC).

RESULTS AND DISCUSSION

Surface Area and Pore Volume Measurement

The nitrogen sorption isotherms for the Cu_3BTC_2 MOF are shown in Figure 2. The sharp uptake of the N_2 gas by the MOF at low relative pressure is an indication of a highly porous structure. The BET surface area, pore size and pore volume of the Cu_3BTC_2 MOF are summarized in Table I. The Cu_3BTC_2 MOF has an average BET surface area of 1777 m^2 g^{-1}, a total pore volume of 0.77 cm^3 g^{-1}, and average pore radius of 0.866 nm. The activation energy of the MOF particle was calculated using eq. (5) with n value (set to 1 based on the adsorption isotherm and the expected activation energy[29]) using Dubinin-Astakhov method. The activation energy was measured to be 44.11 kJ mol^{-1}, which is similar to what has been reported.[30] The high activation energy may be attributed to the formation of coordinate bonds between the metal sites and oxygen atoms present in the water molecules.

$$W = W_o e^{-\left(\frac{-RT\ln P/P_o}{E}\right)^n} \quad (5)$$

where,

W = weight adsorbed at P/P_o and T
W_o = total weight adsorbed
E = characteristic energy
n = noninteger value (typically between 1 and 3)

Figure 2 shows a type I sorption-desorption isotherm, as classified by the international union of pure and applied chemistry. The high adsorption and almost saturated state observed at low relative pressure supports the nanoporous nature of the MOF. The pore volume in this study was calculated at relative pressure of 0.99. BET surface area, pore size, and the pore volume was close to the previously reported values for $Cu_3(BTC)_2$ MOF,[31,32] and the average surface area that was specified by the supplier 1500–2100 m^2 g^{-1}. The pore radius was in range taking the three-dimensional and interior cavity into consideration of 9 × 9 Å.[31]

Scanning Electron Microscopy

Figure 3(a–d) shows SEM images of $Cu_3(BTC)_2$ MOF and PLLA-20% MOF. Permeability and selectivity of the membranes are strongly influenced by the matrix-filler interface. Any microvoids present in the membranes can negatively impact the perm-selectivity due to their nonselective nature. Traditional inorganic compounds used for the fabrication of the MMMs cause generation of micro void at the interface. Natural compatibility exists between MOF particles and polymers because of their hybrid organic-inorganic composition.[21,22,33] SEM studies showed defect free PLLA-MOF interface. Our past study,[27] also, demonstrated strong interfacial interactions between PLLA matrix and $Cu_3(BTC)_2$ MOF particles as observed in the microscopic and rheological studies.

Table I. Surface Area, Pore Volume, and Pore Radius of $Cu_3(BTC)_2$ MOF Calculated from N_2 Isotherm

	Surface area BET (m^2 g^{-1})	Total pore volume (cm g^{-1})	Average pore radius (Å)	Adsorption energy (kJ mol^{-1})
$Cu_3(BTC)_2$	1777 ± 338	0.77 ± 0.14	8.66 ± 0.17	44.11 ± 17.08

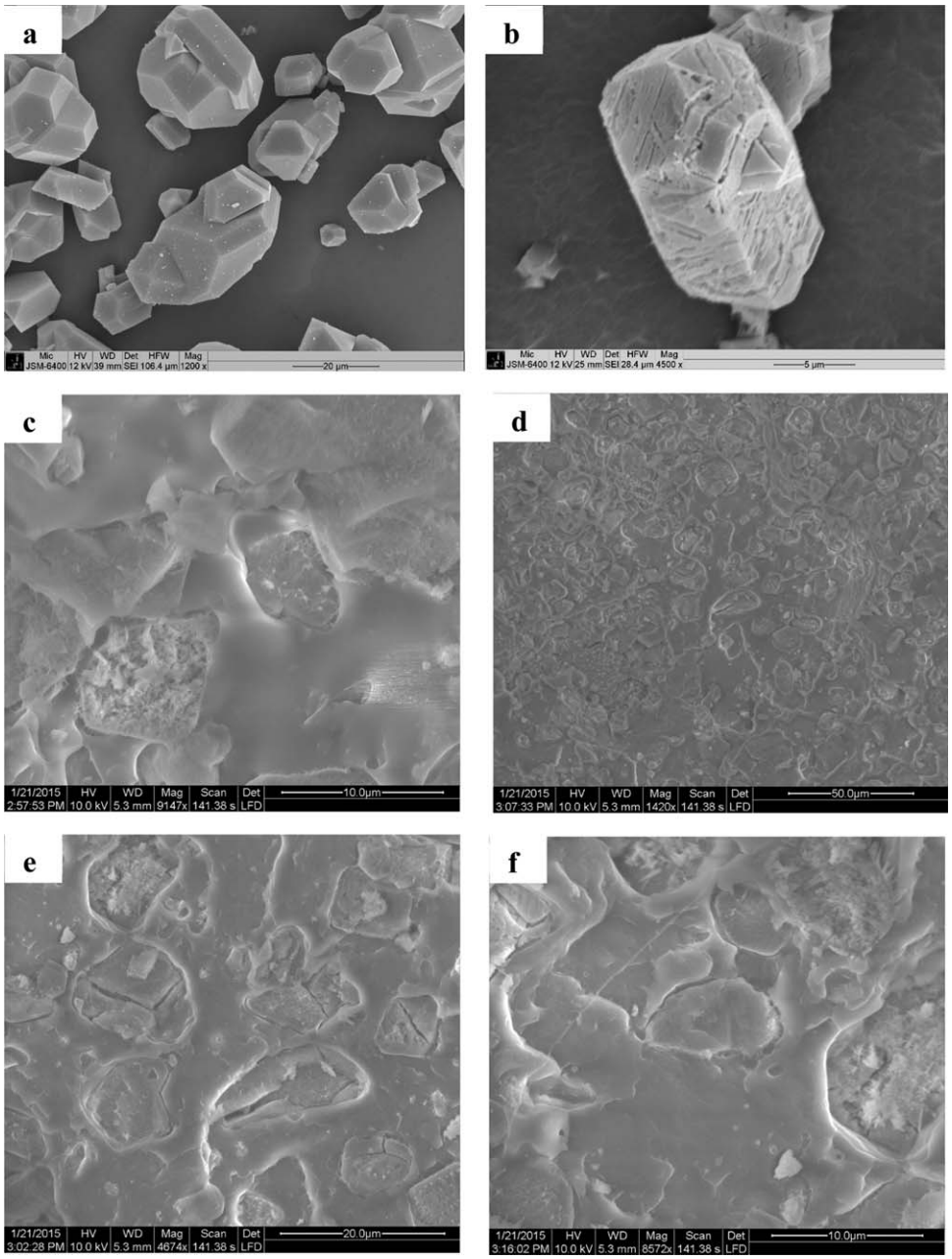

Figure 3. (a) SEM images of $Cu_3(BTC)_2$ MOF scale size 20 μm. (b) SEM image of $Cu_3(BTC)_2$ MOF scale size 5 μm. (c) SEM image of PLLA-20% $Cu_3(BTC)_2$ MOF scale size 10 μm. (d) SEM image of PLLA-20% $Cu_3(BTC)_2$ MOF scale size 50 μm. (e). SEM image of PLLA-$Cu_3(BTC)_2$ MOF scale size 20 μm. (f) SEM image of PLLA-$Cu_3(BTC)_2$ MOF scale size 10 μm.

X-ray Diffraction

Diffractograms of PLLA, $Cu_3(BTC)_2$ MOF, and PLLA-20% $Cu_3(BTC)_2$ MOF composite are represented in Figure 4. The diffraction pattern of PLLA-20% MOF, (Figure 4) shows a wide background peak, which is associated with the amorphous PLLA structure and narrow peaks, which are characteristic of the crystalline $Cu_3(BTC)_2$ MOF. It can be observed from the diffractograms that MOF crystals present in the PLLA matrix diffracted the X rays at same 2θ angles as observed in the activated $Cu_3(BTC)_2$ MOF alone. It indicates that the MOF crystals retained their inherent FCC crystal structure after thermal exposure during the extrusion and injection molding processes. In our previous study,[24] we reported in detail the effect of various processing parameters on the stability of the MOF crystals during the PLLA-MOF membrane fabrication and their effect on the final properties of the membranes. It was observed that activated MOF crystals when melt processed with PLLA retained their crystal structure. However, if there are adsorbed water molecules present in the MOF, the MOF crystal structure can deteriorate during the melt processing and compounding, which can negatively impact the selectivity and gas separation properties of PLLA-$Cu_3(BTC)_2$ MOF based MMMs. Detailed analysis of the effect of water on the thermal stability of PLLA-$Cu_3(BTC)_2$ MOF is reported elsewhere.[24]

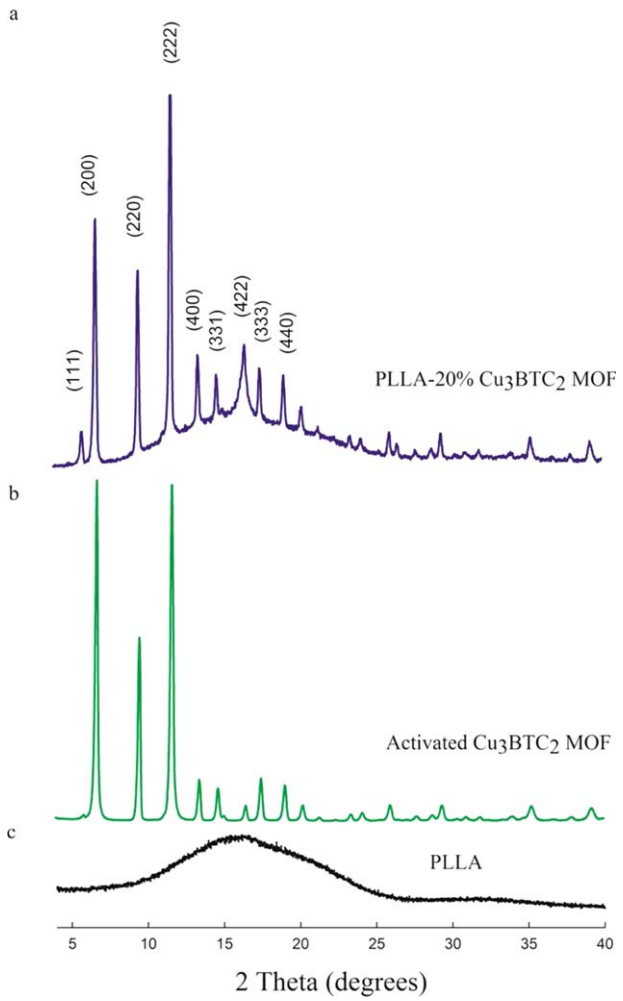

Figure 4. XRD patterns of (a) PLLA-20% $Cu_3(BTC)_2$ MOF; (b) $Cu_3(BTC)_2$ MOF; (c). PLLA. [Color figure can be viewed in the online issue, which is available at wileyonlinelibrary.com.]

Mass Transfer and Perm-Selectivity

CO_2, O_2, H_2O Permeability Coefficient and Perm-Selectivity. Mass transfer properties of MMMs are dependent on the polymeric matrix, MOF crystals, and the final morphology of the composites. Consequently, with varying interfacial interactions between the polymeric matrix and porous filler, MMMs may exist in five different morphologies as shown in Figure 5.[34,35] Figure 5(a) illustrates the ideal defect/distortion free two phase morphology, which exists under good interfacial interactions between the polymer and the porous filler. Figure 5(b) demonstrates the incompatibility between the polymer and the filler, which results in voids at the interface. Figure 5(c) represents the dilated interface, which may be the result of the low density of the polymeric chain around the filler. Figure 5(d) displays a densely packed polymeric zone present around the interface due to strong interactions. In addition to the above mentioned morphologies, there is also the possibility of having plugged filler, which may form during the fabrication of MMMs as indicated in Figure 5(e).

In this study, we used 20% w/w $Cu_3(BTC)_2$ MOF for the fabrication of membranes, the percentage was carefully chosen based on previous studies.[21,24,36] It was observed that with the addition of 20% $Cu_3(BTC)_2$ MOF in the PLLA matrix, CO_2 permeability coefficient increased by around 38% as compared with PLLA. This may be attributed to the favorable quadrupole-quadrupole interactions between the $Cu_3(BTC)_2$ MOF and CO_2.[16,17,22,37,38] Torrisi *et al.*[37,38] reported that the aromatic organic linkers (benzene tri carboxylate) present in the $Cu_3(BTC)_2$ MOF can interact with CO_2 due to strong quadrupole-quadrupole interactions. Basu *et al.*[22] studied CO_2/CH_4 and CO_2/N_2 gas separations using polyimide-$Cu_3(BTC)_2$ MOF based MMMs. They reported an increase in the relative CO_2 permanence of membrane with increase in the $Cu_3(BTC)_2$ MOF loading in the polymer. The authors further attributed this increase to the strong quadrupole moment of CO_2 and poor electrostatic interactions of N_2 and CH_4 molecules with the $Cu_3(BTC)_2$ MOF.

To predict the permeability of MMMs Maxwell and Maxwell Wagner Sillars (MWS) models have been extensively used.[39] The Maxwell model assumes spherical shaped particles for calculating the mass transfer properties of MMMs. The model is represented in eq. (6).

$$PMMM = P_c\left[\frac{P_d+2P_c-2\phi_d(P_c-P_d)}{P_d+2P_c+\phi_d(P_c-P_d)}\right] \quad (6)$$

The MWS model improves on the Maxwell model taking into account the shape factor of the filler particles for calculation of mass transfer [eq. (7)].

$$P_{MMM} = P_c\left[\frac{nP_d+(1-n)P_c+(1-n)(P_d-P_c)\phi_d}{nP_d+(1-n)P_c-n(P_d-P_c)\phi_d}\right] \quad (7)$$

where, P_{MMM} is the permeability of MMM, P_c, and P_d are permeabilities of the continuous phase and dispersed phase, Φ_d is the concentration of filler and n is the shape factor.

Both the experimental and theoretical CO_2 permeability coefficients for PLLA and PLLA-20% MOF MMMs are summarized in Table II. For calculation purposes the CO_2 permeability coefficient of $Cu_3(BTC)_2$ MOF crystals was utilized from a previously reported study[31] and MOF particles were assumed as an oblate spheroid with n equal to 1 for MWS model. According to the MWS model, CO_2 permeability of PLLA-20% $Cu_3(BTC)_2$ MOF increased by almost 89% as compared with the PLLA alone. However, a 38% increase in the CO_2 permeability coefficient of the PLLA with the addition of 20% $Cu_3(BTC)_2$ MOF was measured. This difference between the measured and the calculated permeability can be attributed to densely packed interface of PLLA around the MOF as a result of the strong interfacial interactions between PLLA and the MOF [Figure 5(d)]. This is supported by the increase in crystallinity of PLLA from 2.5 to 11.1% with the addition of 20% MOF. In rheological studies, secondary plateau or terminal shoulder observed at low frequencies in PLLA-20% MOF in G' plots indicate three directional network formation supporting strong interfacial interactions between MOF and PLLA and densely packed interface. Detailed analysis of DSC and rheological studies was reported elsewhere.[27] The irregular shape of the MOF particles; as observed in Figure 3(a); may be another reason for low measured permeability as compared with the model prediction.

The oxygen permeability coefficient and CO_2/O_2 perm-selectivity ($\alpha_{CO2/O2}$) of PLLA and PLLA-20% MOF are presented in Table

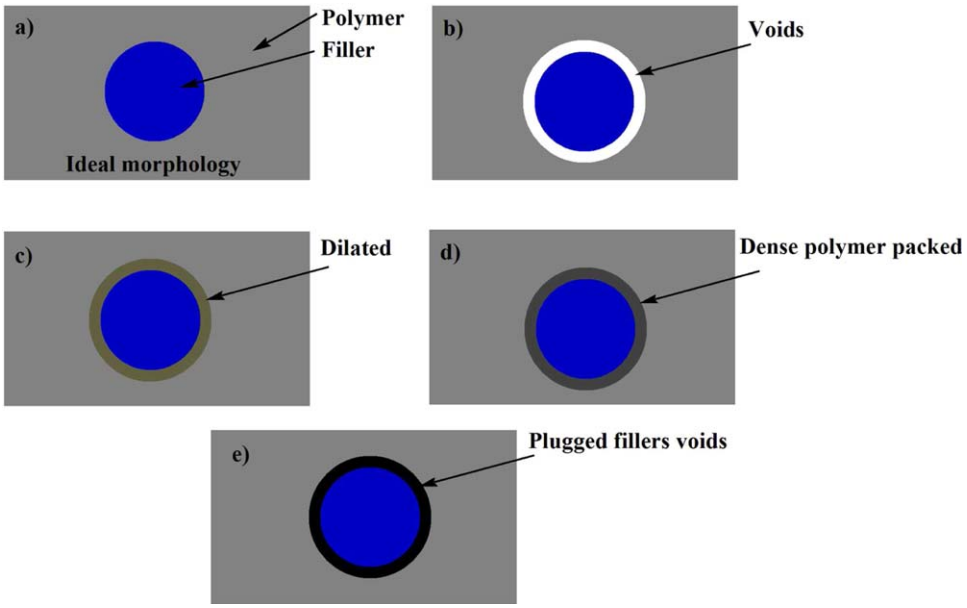

Figure 5. Interfacial morphologies of MMMs (a) Ideal morphology. (b) Interfacial voids. (c) Dilated packed zone around interface. (d) Densely packed zone around interface. (e) Plugged MOF. [Color figure can be viewed in the online issue, which is available at wileyonlinelibrary.com.]

III, there was no statistically significant difference in the oxygen permeability coefficients of PLLA and PLLA-$Cu_3(BTC)_2$ MOF based MMMs, which can be ascribed to poor van der Waals interactions of O_2 molecules with $Cu_3(BTC)_2$ MOF. Supronowicz *et al.*[14] studied that total interaction energies (ΔE_{int}) of CO_2 and O_2 molecules on the under coordinated Cu^{2+} centers of $Cu_3(BTC)_2$ MOF as per hybrid B3lyP density functional theory. They observed that the ΔE_{int} of O_2 and CO_2 molecules are -9.6 and -27.0 kJ mol^{-1}, respectively. Davydovskaya *et al.*[40] studied $Cu_3(BTC)_2$ MOF for sensing and detection of various aldehydes in various atmospheric conditions and concluded that oxygen does not interfere with the detection of aldehydes supporting in turn the hypothesis of poor interactions that exist between MOF and oxygen molecules. The perm-selectivity of PLLA ($\alpha_{CO2/O2}$) improved from 7.6 to 10.3 with the addition of 20% MOF crystals. The increased perm-selectivity can be attributed to the favorable interactions between MOF crystals and CO_2 over O_2.

Water vapor permeability coefficients of PLLA and PLLA-20% MOF are summarized in Table III. The presence of MOF did not affect the water permeability coefficients of PLLA. Strong coordinate bond type interactions and high interaction energy (>40 kJ mol^{-1})[15,16] of H_2O molecules with $Cu_3(BTC)_2$ MOF did not facilitate permeability of the water molecules.

Aroma Permeability Coefficient. Acetaldehyde and trans-2-hexenal considered in this work are made up of a polar functional group consisting of trigonal planar carbon double bond oxygen with an organic chain length of 1.5 and 6.3 Å.[40] Acetaldehyde and trans-2-hexenal have logarithm of octanol water coefficient (Log *P*) of -0.8 and 1.58, respectively.[41,42] A Negative Log *P* value is an indication of the hydrophilic nature of acetaldehyde whereas the positive value correlates to the hydrophobicity of trans-2-hexenal.[41] The permeability coefficients for trans-2-hexenal and acetaldehyde are represented in Table III. Similar permeability coefficient values of both these compounds have been reported previously.[5] Trans-2-hexenal permeability coefficients for PLLA films are higher than those of acetaldehyde. This can be ascribed to the higher solubility coefficients between the hydrophobic PLLA and tran-2-hexenal as supported by Log *P* values. Lee *et al.*[5,43] reported the solubility coefficients of trans-2-hexenal and acetaldehyde as 55.89 and 19.5 kg m^{-3} Pa^{-1}, respectively.

We observed a 60% increase in the trans-2-hexenal permeability coefficient with the addition of 20% MOF to the PLLA matrix. However, no change in the mass transfer of acetaldehyde was observed in PLLA-20% MOF matrix as compared to neat PLLA films. The difference in mass transfer rates of the two aldehydes may be explained by: (i) the influence of the existing

Table II. Theoretical and Experimental CO_2 Permeability Coefficient of PLLA and PLLA-20% MOF Composites

	Permeability coefficient × 10^{-18} (kg m m^{-2} s^{-1} Pa^{-1})		
		Theoretical predictions	
	Experimentally observed	Maxwell model	MWS model
PLLA	45.54 ± 2.72^a	45.54	45.54
PLLA-20% MOF	63.03 ± 1.86^b	167.47	86.19

Note: Values in the same column with same lower case superscript alphabets are not statistically significantly different at $\alpha = 0.05$.

Table III. Trans-2-Hexenal, Acetaldehyde, H_2O, CO_2, O_2 Permeability Coefficients, and CO_2/O_2 Permselectivity of PLLA and PLLA-20% MOF Composites

	Permeability coefficient × 10^{-14} (kg m m^{-2} s^{-1} Pa^{-1})			Permeability coefficient × 10^{-18} (kg m m^{-2} s^{-1} Pa^{-1})		Permselectivity
	Trans-2-hexenal	Acetaldehyde	H_2O	CO_2	O_2	$\alpha_{CO2/O2}$
PLLA	29.21 ± 1.56[a]	15.3 ± 3.93[a]	3.29 ± 0.31[a]	45.54 ± 2.72[a]	6.00 ± 0.40[a]	7.59
PLLA-20% MOF	46.99 ± 2.36[b]	15.4 ± 0.80[a]	3.28 ± 0.23[a]	63.03 ± 1.86[b]	6.14 ± 0.87[a]	10.26

Note: Values in the same column with same lower case superscript alphabets are not statistically significantly different at $\alpha = 0.05$.

environmental conditions during testing (relative humidity and temperature); (ii) the effect of the carbon chain length attached to the aldehyde functional group; and (iii) the aldehyde's polarity and geometry. Moreover, the increase in the trans-2-hexenal permeability coefficient may also be attributed to a physisorption type interaction between trans-2-hexenal and Cu_3BTC_2 MOF occurring under favorable humidity conditions (50% RH).[40]

Davydovskaya *et al.*[40] studied the sensing of various aldehydes with different chain length using work function based Cu_3BTC_2 sensor. They observed that in the case of pentanal the sensing capability of Cu_3BTC_2 sensor improved with increasing humidity from 28 to 42% RH. However, no further improvement in signal was observed with any additional increase in humidity beyond 42%. This indicates that humidity plays a very important role in the interaction of aldehydes with Cu_3BTC_2 MOF. Although the exact mechanism is still not well understood, the difference in the behavior of mass transfer properties of PLLA-20% Cu_3BTC_2 MOF MMMs toward acetaldehyde and tran-2-hexanal may be attributed to the fact that the acetaldehyde mass transfer was studied using GC studies conducted using a jar in which film is exposed to a controlled environment free of humidity, thus isolating the membranes from environmental humidity. However, in the tran-2-hexanal studies, the films were exposed to 23°C and 50% RH.

In addition, the polar group attached to two carbons and four hydrogens in acetaldehyde is more dominant in the overall structure as compared to trans-2-hexanal in which the polar group is attached to six carbon atoms. Dominant polar structure and small molecular size of acetaldehyde may have helped in chelation/complex formation between the oxygen atom of acetaldehyde with the unsaturated copper sites present in the $Cu_3(BTC)_2$ MOF under dry atmospheric conditions as shown in Figure 6. The stronger chemisorption interaction contributes to the binding of the organic or gaseous molecule to the Cu metal site. Once these open metal sites are occupied by the chemisorbed acetaldehyde, it is hard to remove these molecules from these pore sites and the MOF will not abet the mass transfer/permeability of these organic or gaseous molecule species.

Gel Permeation Chromatography

The molecular weight (M_w) and molecular weight distribution (MWD) can have significant impact on the mass transfer properties of the polymeric materials and composites. In order to understand the effect of MOF particles on any possible changes in the molecular weight GPC studies were performed. Chromatography studies indicate that PLLA retained its molecular structure and molecular weight after the thermal exposure during extrusion processing with MOF. There was no significant difference in the number average molecular weight of PLLA and PLLA-20% MOF. Although there is a statistical difference in the weight average molecular weight of the PLLA and PLLA-20% MOF samples, the difference is minimal and could be associated with the material variation in the molecular weight of resin supplied by the manufacturer. M_w and MWD did not affect the mass transfer properties of the MMMs in this study (Table IV).

This study demonstrated that the MOF particles can influence the mass transfer rate of various gases and volatile compounds which has implications for various applications including food

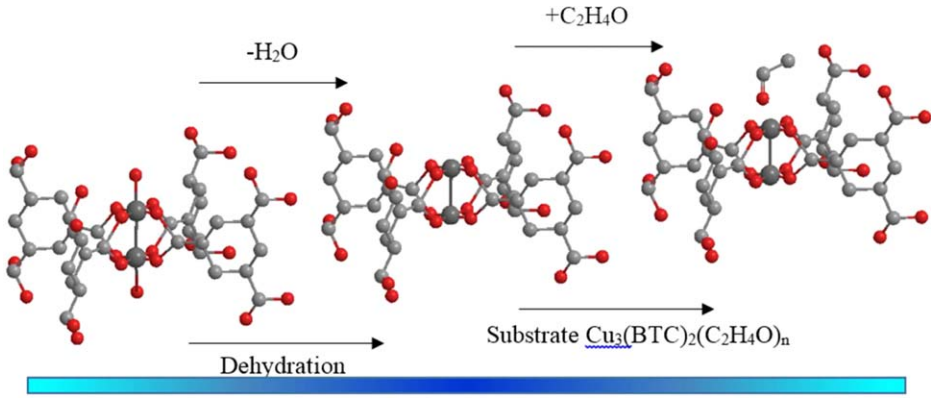

Figure 6. Chemisorption of acetaldehyde in $Cu_3(BTC)_2$ MOF structure after dehydration, dark gray; Cu atoms, light gray; carbon, red; oxygen atom, and hydrogen atoms omitted. [Color figure can be viewed in the online issue, which is available at wileyonlinelibrary.com.]

Table IV. Molecular Weight of PLLA and PLLA-20% MOF Composites

	M_n (kDa)	M_w (kDa)	PDI
PLLA	71.9 ± 1.2^a	103.0 ± 0.7^a	1.4 ± 0.0^a
PLLA-20% MOF	71.7 ± 3.8^a	107.1 ± 1.7^b	1.5 ± 0.1^a

Note: Values in the same column with same lower case superscript alphabets are not statistically significantly different at $\alpha = 0.05$.

packaging. Future work will concentrate on assessing additional mass transfer properties of the PLA MOF membranes and determining the migration/release of cooper from the developed membranes.

CONCLUSIONS

According to this study, it was observed that the CO_2/O_2 permselectivity ($\alpha_{CO2/O2}$) of PLLA films increases with the addition of 20% (w/w) $Cu_3(BTC)_2$ MOF. The increased carbon dioxide and trans-2-hexenal permeabilities can be associated with strong physisorption (quadrupole-quadrupole) type interaction between the gas molecules and the MOF. Aromatic or water molecules with ability to chemically coordinate on the metal sites in the MOF did not show any changes in the mass transfer properties. The presence of nanoporous MOF crystals in the polymeric matrices can significantly influence the barrier properties of certain gases and organic aromatic compounds; depending on the nature of interactions with these molecules; providing a gamut of opportunities in fields, such as gas separation, energy and packaging.

ACKNOWLEDGMENTS

RA would like to acknowledge the support of the USDA National Institute of Food and Agriculture and Michigan AgBioResearch, Hatch project R. Auras.

REFERENCES

1. Auras, R. A.; Harte, B.; Selke, S.; Hernandez, R. J. *J. Plast. Film* **2003**, *19*, 123.
2. Bao, L.; Dorgan, J. R.; Knauss, D.; Hait, S.; Oliveira, N. S.; Maruccho, I. M. *J. Membr. Sci.* **2006**, *285*, 166.
3. Auras, R.; Harte, B.; Selke, S. *Macromol. Biosci.* **2004**, *4*, 835.
4. Lehermeier, H. J.; Dorgan, J. R.; Way, J. D. *J. Membr. Sci.* **2001**, *190*, 243.
5. Almenar, E.; Auras, R. In Poly(lactic acid) Synthesis, Structures, Properties, Processing, and Applications; Auras, R., Lim, L. T., Selke, S. E. M., Tsuji, H., Eds.; Wiley: New York, **2010**; Chapter 12, p 155.
6. Tsuji, H.; Tsuruno, T. *Macromol. Mater. Eng.* **2010**, *8*, 709.
7. Eddaoudi, M.; Moler, D. B.; Li, H.; Chen, B.; Reineke, T. M.; O'Keeffe, M.; Yaghi, O. M. *Acc. Chem. Res.* **2001**, *34*, 319.
8. Rosi, N. L.; Eckert, J.; Eddaoudi, M.; Vodak, D. T.; Kim, J.; O'Keeffe, M.; Yaghi, O. M. *Science* **2003**, *300*, 1127.
9. Rowsell, J. L. C.; Yaghi, O. M. *Angew. Chem. Int. Ed.* **2005**, *44*, 4670.
10. Zhuang, W.; Yuan, D.; Li, J. R.; Luo, J.; Zhou, H. C.; Bashir, S.; Liu, J. *Adv. Healthc. Mater.* **2012**, *1*, 225.
11. Prestipino, C.; Regli, L.; Vitillo, J. G.; Bonino, F.; Damin, A.; Lamberti, C.; Zecchina, A.; Solari, P. L.; Kongshaug, K. O.; Bordiga, S. *Chem. Mater.* **2006**, *18*, 1337.
12. Wang, Z.; Cohen, S. M. *J. Am. Chem. Soc.* **2007**, *129*, 12368.
13. Eddaoudi, M.; Kim, J.; Rosi, N.; Vodak, D.; Wachter, J.; O'Keeffe, M.; Yaghi, O. M. *Science* **2002**, *295*, 469.
14. Millward, A. R.; Yaghi, O. M. *J. Am. Chem. Soc.* **2005**, *51*, 17998.
15. Küsgens, P.; Rose, M.; Senkovska, I.; Fröde, H.; Henschel, A.; Siegle, S.; Stefan, K. *Microporous Mesoporous Mater.* **2009**, *120*, 325.
16. Castillo, J. M.; Vlugt, T. J. H.; Calero, S. *J. Phys. Chem. C* **2008**, *112*, 15934.
17. Supronowicz, B.; Mavrandonakis, A.; Heine, T. *J. Phys. Chem.* **2013**, *117*, 14570.
18. Sen, D.; Kalýpcýlar, H.; Yilmaz, L. *J. Memb. Sci.* **2007**, *303*, 194.
19. Ahn, J.; Chung, W. J.; Pinnau, I.; Guiver, M. D. *J. Memb. Sci.* **2008**, *314*, 123.
20. Bertelle, S.; Gupta, T.; Roizard, D.; Vallières, C.; Favre, E. *Desalination* **2006**, *199*, 401.
21. Adams, R.; Carson, C.; Ward, J.; Tannenbaum, R.; Koros, W. *Microporous Mesoporous Mater.* **2010**, *131*, 13.
22. Basu, S.; Cano-Odena, A.; Vankelecom, I. F. *J. Memb. Sci.* **2010**, *362*, 478.
23. Chui, S. S. Y.; Lo, S. M.-F.; Charmant, J. P. H.; Orpen, A. G.; Willaims, I. D. *Science* **1999**, *283*, 1148.
24. Kathuria, A.; Abiad, M.; Auras, R. *Polym. Int.* **2013**, *62*, 1144.
25. Li, H.; Eddaoudi, M.; O'Keeffe, M.; Yaghi, O. M. *Nature* **1999**, *402*, 276.
26. Rowsell, J. L. C.; Yaghi, O. M. *Microporous Mesoporous Mater.* **2004**, *73*, 3.
27. Kathuria, A.; Abiad, M.; Auras, R. *Polymer* **2013**, *54*, 6979.
28. Dorgan, J. R. In Poly(Lactic Acid): Synthesis, Structures, Properties, Processing, and Applications; Auras, R., Lim, L., Selke, S., Tsuji, H., Eds.; Wiley: New York, **2010**; Chapter 10, pp 125.
29. Terzyk, A. P.; Gauden, P. A.; Kowalczyk, P. *Carbon* **2002**, *40*, 2879.
30. Stoeckli, H. F. *Carbon* **1990**, *28*, 1.
31. Guo, H.; Zhu, G.; Hewitt, I. J. *J. Am. Chem. Soc.* **2009**, *131*, 1646.
32. Krawiec, P.; Kramer, M.; Sabo, M.; Fröde, H.; Kaske, S. *Adv. Eng. Mater.* **2006**, *8*, 293.
33. Ren, H. Q.; Jin, J.; Hu, J. *Ind. Eng. Chem. Res.* **2012**, *51*, 10156.
34. Adams, R.; Johnson, J. R.; Zhang, C.; Lively, R.; Dai, Y.; Esekhile, O.; Liu, J.; Koros, W. J. In Encyclopedia of Membrane Science and Technology; Hoek, M. V., Tarabara, V. V., Eds.; Wiley: New York, **2013**; Vol. 3, Part II. Mixed Matrix Membranes, pp 1.
35. Vinh-Thang, H.; Kaliaguine, S. *Chem. Rev.* **2013**, *113*, 4980.

36. Elangovan, D.; Nidoni, U.; Yuzay, I. E.; Selke, S. E. M.; Auras, R. *Ind. Eng. Chem. Res.* **2011**, *50*, 11136.

37. Torrisi, A.; Mellot-Draznieks, C.; Bell, R. G. *J. Chem. Phys.* **2009**, *130*, 194703.

38. Torrisi, A.; Mellot-Draznieks, C.; Bell, R. G. *J. Chem. Phys.* **2010**, *132*, 044705.

39. Gonzo, E. E.; Parentis, M. L.; Gottifredi, J. C. *J. Membr. Sci.* **2006**, *277*, 46.

40. Davydovskaya, P.; Pohle, R.; Tawil, A.; Fleischer, M. *Sens. Actuator B* **2013**, *187*,142.

41. Espinosa-Diaz, M.; Seuvre, A. M.; Voilley, A. In Flavor Science: Recent Developments; Taylor, A. J., Mottram, D. S., Eds.; Wiley: New York, **2013**; Section 7, p 442.

42. Naknean, P.; Meenune, M. *Int. Food Res. J.* **2010**, *17*, 23.

43. Lee, R.; Almenar, E.; Auras, R.; Harte, J.; Harte, B.; Rubino, M. Characterization of Poly(lactic acid) Sheet During and After Exposure to Main Aroma Compounds of Foods, in: Polymers and the Environment-Emerging Technologies and Science Annual Meeting, Chicago, IL, **2009**.